Journal of Sound and Vibration (2002) **258**(1), 31–44
doi:10.1006/jsvi.5070, available online at http://www.idealibrary.com on IDEAL®

COMPLEX DYNAMICS OF HIGH-SPEED AXIALLY MOVING SYSTEMS

F. Pellicano

Dipartimento di Ingegneria Meccanica e Civile, Università di Modena e Reggio Emilia, Via Vignolese 905, 41100 Modena, Italy. E-mail: frank@unimo.it

and

F. Vestroni

Dipartimento di Ingegneria Strutturale e Geotecnica, Università di Roma "La Sapienza", Via Eudossiana 18, 00184 Rome, Italy. E-mail: vestroni@uniroma1.it

(*Received* 17 *January* 2001, *and in final form* 14 *November* 2001)

In this paper, the dynamic response of a simply supported travelling beam subjected to a transverse load is investigated in the super-critical speed range. The well-known axially moving beam theory is considered and a simple viscous damping mechanism has been introduced. The displacement field is expanded in a series of the buckling modes, a sine series, and different techniques have been used in analyzing the response of the dynamical system. Periodic oscillations are studied by means of continuation techniques, while non-stationary dynamics are investigated through direct simulations. A comparison with the literature and a convergence test on the series expansion are performed. A sample case of a physical beam is developed and numerical results are presented concerning bifurcation analysis and stability, and direct simulations of global postcritical dynamics. A complex scenario of alternate regular and chaotic motions is found in a large range of the main parameters.

1. INTRODUCTION

The wide diffusion of axially moving systems in industrial processes has motivated intense research activity, which began in the middle of the last century. Power transmission belts, paper sheet processes, aerial cables, and magnetic tapes, are only some examples of one-dimensional continua where vibrations are associated with an axial transport of mass. In these systems the axial speed plays an important role in changing the elastic behavior of the beam; the centrifugal forces associated with the curvature and the axial speed decrease the stiffness of the beam, the Coriolis forces associated with the rotation and the axial speed give rise to travelling wave modes of vibration. Moreover, above a certain critical velocity, the first frequency of the system becomes zero: the straight equilibrium configuration becomes unstable and bifurcates in multiple equilibrium positions.

The literature regarding axially moving systems is wide, in references [1, 2] an extensive literature overview can be found. In the following the most interesting works, strictly related to the present paper, are commented on.

In reference [3] the vibrations of finite and infinite moving threadlines have been studied and the effect of the axial velocity on the linear frequencies is qualitatively discussed, while

0022-460X/02/$35.00

in reference [4] the role of non-linearities in a travelling string and the effect of axial velocity received particular attention. In reference [5] a special modal analysis for axially moving beams/strings has been developed and some features of these systems were reanalyzed. Moreover, the Green function was obtained in terms of the analytical eigenfunctions. It is also found that some stability regions exist in the super-critical speed range, i.e., in specific intervals of the super-critical speed range the trivial equilibrium position regains stability.

The fundamental role of non-linearity for high-speed systems has been widely ascertained in studies on the non-linear vibrations and bifurcations of moving beams [3, 4, 6, 7] which are strictly related to the subject of the present work. In reference [6] bifurcation and stability are analyzed, and the non-linear response, in sub- and super-critical speed ranges, is examined by means of local analyses, i.e., singular perturbation techniques; in particular, the existence of a global motion around the critical speed was predicted. Hwang and Perkins [8, 9] investigated the effect of an initial curvature due to supporting wheels and pulleys on the bifurcation and stability of equilibrium; they underlined the system sensitivity to initial imperfections. In references [2, 10] a high-dimensional discrete model obtained by a Galerkin procedure is developed, and linear stability and non-linear free undamped oscillations are analyzed.

In the present work, the discrete technique proposed in reference [2] is used to study the response of an axially moving beam subjected to harmonic excitation. The resulting finite-dimensional dynamical system contains a linear part with symmetric mass and stiffness matrices, a skew-symmetric gyroscopic matrix, a cubic non-linearity and a simple viscous damping. The spectral analysis of the linear part of the discrete system provides imaginary eigenvalues and complex eigenvectors [2], according to the available analytical results [5, 6]. The straight equilibrium configuration exhibits a pitchfork bifurcation at the critical value of speed. Here, the attention is focused on the postbifurcation velocity range, in the presence of viscous damping and external harmonic excitation. Periodic oscillations are analyzed by means of the code AUTO [11], which is based on a collocation method and is able to follow periodic solutions, their stability and bifurcations, when a system parameter is varied. Non-stationary dynamics are analyzed with a fourth to fifth order adaptive step size Runge–Kutta algorithm. Time histories, Fourier spectra, Poincaré maps and their bifurcation diagrams are used to analyze the response of the dynamical system. A first analysis is performed on the same problem studied in reference [6], in order to perform comparisons between the Galerkin approach proposed and results available in the literature. Convergence tests are developed to quantify the minimum number of degrees of freedom (d.o.f) needed to describe the displacement field accurately. A detailed analysis of periodic and chaotic regimes, which is the main objective of the present work, is focused on exploring the system dynamics when its main parameters vary.

2. EQUATION OF MOTION

Axially moving systems are studied by means of a simply supported beam model with fixed ends, where the axial transport of mass and the non-linear coupling between longitudinal and transversal displacement fields is accounted for. Although the physical model of a beam with supported fixed ends is very simple, the results furnished by this model are consistent with real problems, as confirmed by a good agreement between theoretical and experimental results, obtained in references [12, 13] using the same model.

For this model the non-dimensional equation of motion reads as

$$\frac{\partial^2 w}{\partial t^2} + 2v\frac{\partial^2 w}{\partial x \partial t} + (v^2 - 1)\frac{\partial^2 w}{\partial x^2} + v_f^2 \frac{\partial^4 w}{\partial x^4} = \frac{v_T^2}{2}\frac{\partial^2 w}{\partial x^2}\int_0^1 \left(\frac{\partial w}{\partial \sigma}\right)^2 \mathrm{d}\sigma + f\cos\omega t\,\delta(x - x^*) \tag{1a}$$

with the relevant boundary conditions:

$$w(0,t) = w(1,t) = 0, \quad \frac{\partial^2 w}{\partial x^2}(0,t) = \frac{\partial^2 w}{\partial x^2}(1,t) = 0, \tag{1b}$$

where $w = \tilde{w}/\ell$, $x = \tilde{x}/\ell$, $t = \tilde{t}\sqrt{P/\rho A \ell^2}$, $v = \tilde{v}/\sqrt{P/\rho A}$, $v_T = \sqrt{EA/P}$, $v_f = \sqrt{EI/P\ell^2}$, $f = \tilde{f}/(P/\ell)$ and $\delta(x)$ is the Dirac function, ℓ the beam length, $\tilde{x}$ the axial co-ordinate, $\tilde{w}$ the transverse displacement field, $\tilde{t}$ the dimensional time, $\tilde{v}$ the longitudinal velocity, P the axial pre-load, ρ the mass density, A the cross-sectional area, E Young's modulus, I the second moment of area of the cross-section, $\tilde{f}$ is the value of point-wise excitation at $x = x^*$. The terms: $2v\partial^2 w/\partial x \partial t$ and $v^2\partial^2 w/\partial x^2$ are the Coriolis force and the centrifugal force, respectively, while the remaining inertial and elastic terms are well known in beam–string theory.

The Coriolis term plays an important role in introducing a skew-symmetric part into the differential operator and transforming the normal modes from real ($\tilde{v} = 0$) to complex ($\tilde{v} \neq 0$), i.e., travelling wave modes. The integral term arises from a classical static condensation of longitudinal displacement, where the fast dynamics in the longitudinal direction is neglected [2, 6, 7].

The centrifugal term produces a decrease in the linear natural frequencies as the axial velocity increases and is responsible for pitchfork bifurcation. When the axial speed of the beam is large enough, the centrifugal forces can exceed the elastic forces and the trivial equilibrium position $w(x,t) = 0$ can become unstable. Analytical formulae for fixed points of equation (1) and critical speed are available [6]: $w^{(k)}(x) = \pm(2/k\pi v_T)\sqrt{v^2 - v^{(k)2}}$, $k = 1, \ldots$; $v^{(k)} = \sqrt{1 + (k\pi v_f)^2}$; $v > v^{(k)}$. From a static point of view the travelling beam behaves as a compressed beam. The effect of the velocity and, in particular, the gyroscopic forces change the postcritical dynamic behavior: they stabilize the trivial equilibrium position in a certain range of speed values, and also provide important linear coupling.

3. DISCRETE MODEL

In the analysis of the non-linear oscillations of a continuous system, the partial differential equations and the relevant boundary conditions are usually reduced to a low-dimensional system of ordinary differential equations, using a spatial representation in terms of a limited number of functions, which should be suitably selected in order to represent the coupling non-linear phenomena under study. Typically, few eigenfunctions of the linearized problem are considered; however, a strong reduction in the phase space leads to a discrete model, which could give unsatisfactory results and sometimes is not able to describe the non-linear phenomenon correctly. In order to reduce the approximation of truncation, different methods have been developed in the past. They are based on the center manifold theorem, on the concept of non-linear normal modes, on vector bases suitably selected from experimental or numerical responses of the system, and direct perturbation techniques. These reduction methods are referred to, for examples, in references [14–17]. It is worthwhile to note that the general Cauchy problem was fully considered in reference [18] for free non-linear oscillations of thin axially moving beams.

Here, no model reduction is intended to be pursued and no reference is made to the previously mentioned methods. The displacement field $w(x,t)$ is expanded in a series of suitable functions $\varphi_n(x)$, truncating the series at the Nth term, but without any restriction on N, using the Galerkin procedure. The basis $\varphi_n(x)$ must be a complete set of functions of the Hilbert space. This implies that the boundary conditions must also be respected; here the sine series is selected:

$$w(x,t) = \sum_{n=1}^{N} q_n(t) \sin n\pi x. \tag{2}$$

Even though the eigenfunctions of the linearized problem often give faster convergence, the use of sine series, which are eigenfunctions for $v = 0$ only, is motivated by the following considerations: (1) the eigenfunctions are not available analytically, they must be numerically evaluated for each axial speed, and parametric studies become difficult; (2) after the bifurcation, multiple equilibrium states are present, each equilibrium position defines a set of eigenfunctions and, for a global motion around more than one position, there is no sense referring to eigenfunctions, moreover, the use of eigenfunctions after the bifurcation can lead to lack of convergence [19]; (3) the sine series easily allows a high-dimensional phase space to be developed, with simple analytical dependence on the speed; (4) sine functions represent the bifurcation modes, i.e., they have a clear physical meaning.

The number of functions N, in equation (2), depends on the convergence of the sine series and is linked to the smoothness of the function $w(x,t)$. In the Galerkin method series (2) is substituted in equation (1a), both terms of the equation are multiplied by $\sin k\pi x$, $k = 1,\ldots,N$, and the result is then integrated over the domain [0,1]. After this projection, a finite-dimensional dynamical system is obtained

$$\ddot{\mathbf{q}} + \mathbf{C}\dot{\mathbf{q}} + \mathbf{K}\mathbf{q} = \mathbf{N}(\mathbf{q}) + \mathbf{f}(t), \tag{3}$$

where $\mathbf{C}$ is made up of a gyroscopic matrix and a diagonal viscous modal matrix, which represents the dissipation effect, $\mathbf{K}$ is the stiffness matrix, $\mathbf{f}(t) = (f_1, f_2, \ldots, f_N)^{\mathrm{T}}$, $f_n(t) = 2f \sin \pi x * \cos \omega t$. Details of equation (3) are fully described in reference [2].

The term $\mathbf{N}(\mathbf{q})$ collects the non-linearities and is defined by applying the Galerkin method to equation (1a). Due to the presence of a skew-symmetric matrix, it is convenient to rewrite the equations in the state space:

$$\dot{\mathbf{p}} = \mathbf{A}\mathbf{p} + \mathbf{F}(\mathbf{p}, t), \tag{4}$$

where $\mathbf{p} = (\dot{\mathbf{q}}^{\mathrm{T}}, \mathbf{q}^{\mathrm{T}})^{\mathrm{T}}$,

$$\mathbf{A} = \begin{bmatrix} \mathbf{C} & \mathbf{K} \\ \mathbf{I} & \mathbf{0} \end{bmatrix}, \quad \mathbf{F}(\mathbf{p}, t) = -[(\mathbf{N}(\mathbf{q}) + \mathbf{f}(t))^{\mathrm{T}}, \mathbf{0}]^{\mathrm{T}}.$$

The matrix $\mathbf{A}$ is the linear operator describing the dynamics of the system in the neighborhood of the trivial equilibrium position $w(x,t) = 0$. The spectral analysis of this operator furnishes the linear frequencies and mode shapes, and allows the stability of the equilibrium position to be evaluated [2].

4. ANALYTICAL INVESTIGATIONS

4.1. COMPARISONS WITH AVAILABLE RESULTS

The non-linear dynamics of axially moving beams are studied in reference [6] by means of perturbation techniques applied directly to the partial differential equations. Assuming a linear eigenfunction as the zero order solution, a non-linear normal mode was analyzed,

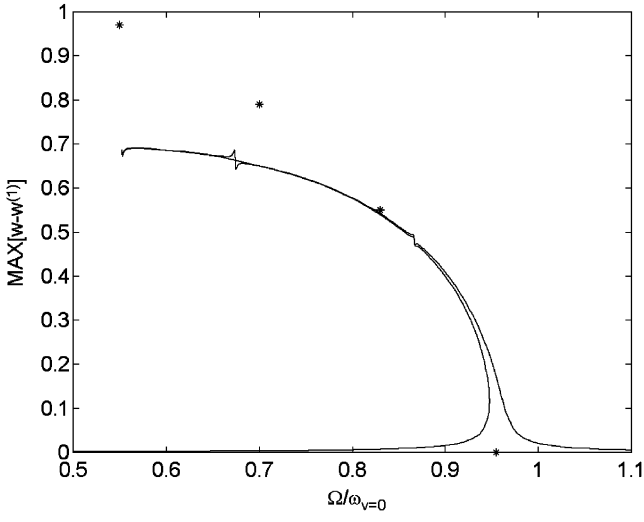

Figure 1. Comparison between the Wickert [6] solution (*) and the present numerical solution (——), for $v_f = 1$, $v_T = 1$, $v/v_{cr} = 1{\cdot}3$, $v_{cr} = 3{\cdot}2969$, $w^{(1)} = 1{\cdot}7435$. For the numerical solution: $f = 10^{-3}$, damping ratio equal to 10^{-3}.

in particular, backbone curves were obtained. The numerical techniques used in the present work are not suitable for finding free monofrequent oscillations. However, it is well known that the backbone curve is the limit of the amplitude frequency curve, when the external excitation is harmonic, its frequency is close to the linear natural frequency considered and both excitation amplitude and viscous damping tend to zero. In Figure 1 large amplitude oscillations around the bifurcated equilibrium position are analyzed, the backbone curve by the Wickert solution [6] is compared with the present numerical results obtained with the software AUTO [11]. It is interesting to note that the present solution is very close to the Wickert solution up to an amplitude of the order of 60% of the beam length, after this level the numerical solution becomes more softening. Moreover, some peaks are visible in the numerical solutions; such irregular behavior is expected when the orbit passes in the vicinity of another equilibrium position. In this case the interaction with the unstable trivial equilibrium position is present. The difference between the numerical results and those given in reference [6], is not surprising, since the asymptotic techniques as used in reference [6], give accurate results when the amplitude is moderately large and the motion is local.

4.2. CONVERGENCE TESTS

A convergence test on the sine series used in expanding the displacement field is performed. The following physical case is studied: $\ell = 0{\cdot}2\,\mathrm{m}$, $A = 10^{-5}\,\mathrm{m}^2$, $I = 2{\cdot}08 \times 10^{-13}\,\mathrm{m}^4$, $E = 2{\cdot}1 \times 10^{11}\,\mathrm{N/m}^2$, $P = 100\,\mathrm{N}$, which can model a saw blade system; the corresponding non-dimensional quantities in the equation of motion are $v_f = 0{\cdot}104$, $v_T = 145$ and the first critical non-dimensional velocity is $v^{(1)} = 1{\cdot}05$. In the numerical analysis large coefficients, such as $v_T = 145$, can give numerical troubles. In order to avoid these problems the following parameterization is introduced: $q_n = \beta \hat{q}_n$ and $\hat{f} = f/\beta$ is the new non-dimensional force and the parameter β is assumed equal to 0·0069 in the simulations. The symbol "$\hat{}$" will be dropped in the following.

Two test cases are considered: (1) regular motion in a super-critical speed range, $v = 1{\cdot}1$ with $f = 0{\cdot}035$, $\omega = 0{\cdot}3$, damping ratio 0·02; (2) chaotic motion in a super-critical speed range, $v = 1{\cdot}1$ with $f = 0{\cdot}54$, $\omega = 0{\cdot}567$, damping ratio 0·02. A detailed analysis of the periodic and chaotic regions will be performed in the next two sections. In Figures 2(a) and 2(b), time histories and spectra obtained by using $N = 1, \ldots, 8$ and 12 are presented, for case (1). When $N > 3$ both time histories and spectra become close to each other, showing that the convergence is rapid. The responses obtained with $N = 1, \ldots, 8$ are compared with the 12 d.o.f. model in the frequency domain (fast fourier transform). In Figure 2(c) a bar chart reports the percentage differences between the low-dimensional models and the 12 d.o.f. discretization. It is clear that for $N > 3$ the percentage difference, here called error, approaches zero and the expansion is convergent. In Figures 3(a) and 3(b) time histories and spectra obtained using $N = 1$, 2, 4, 8 and 12 are presented, for case (2). When $N > 4$ both time histories and spectra become close to each other; here the convergence is slower. The cases $N = 1$, 2, 4, 8 are compared with the 12 d.o.f. model, in the frequency domain (power spectral density); in Figure 3(c) a bar chart reports the percentage differences between the low-dimensional models and the 12 d.o.f. discretization. Note that the error, for the case $N = 1$, is higher than 100%. When $N > 4$ the difference becomes small and the series expansion is close to convergence. For case (2) the power spectral density is used instead of the classical FFT, because the chaotic signals

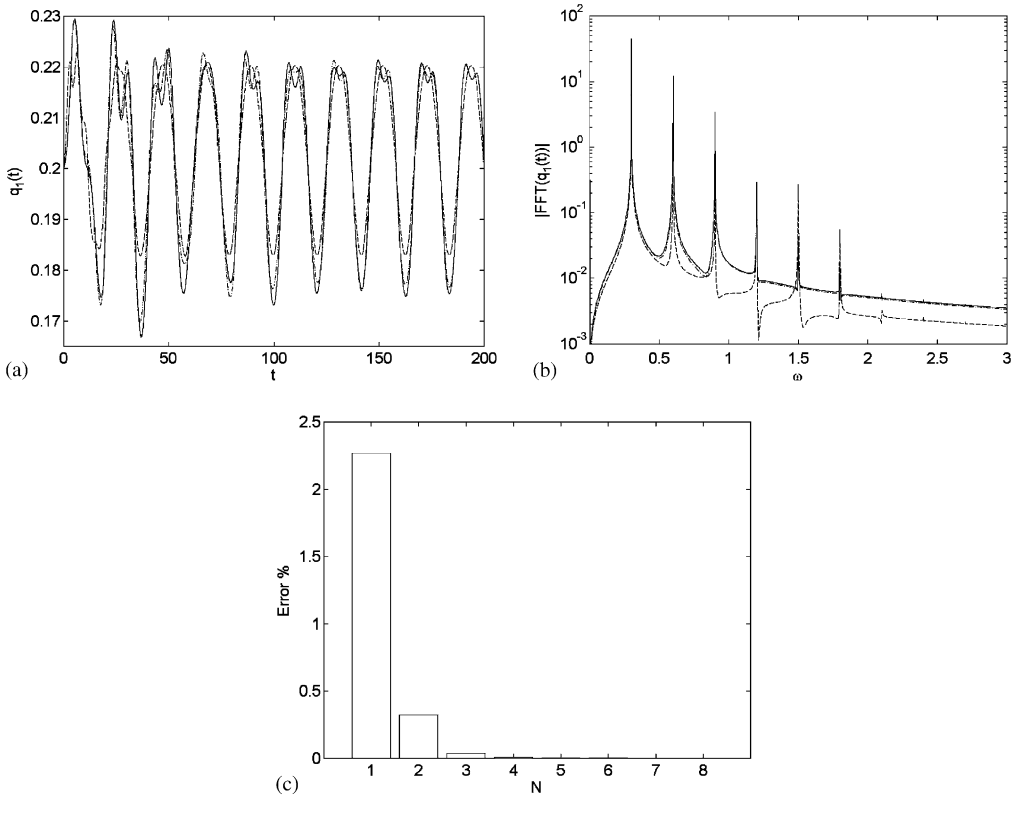

Figure 2. Regular motion: (a) time history for $f = 0{\cdot}035$, $\omega = 0{\cdot}3$, $v = 1{\cdot}1$; (b) spectra of signals. - - - -, 1 d.o.f.; -·-·-·-, 2 d.o.f.; ·····, 3 d.o.f.; ——, $n > 3$ d.o.f.; (c) percent spectral error with respect to the 12 d.o.f. solution.

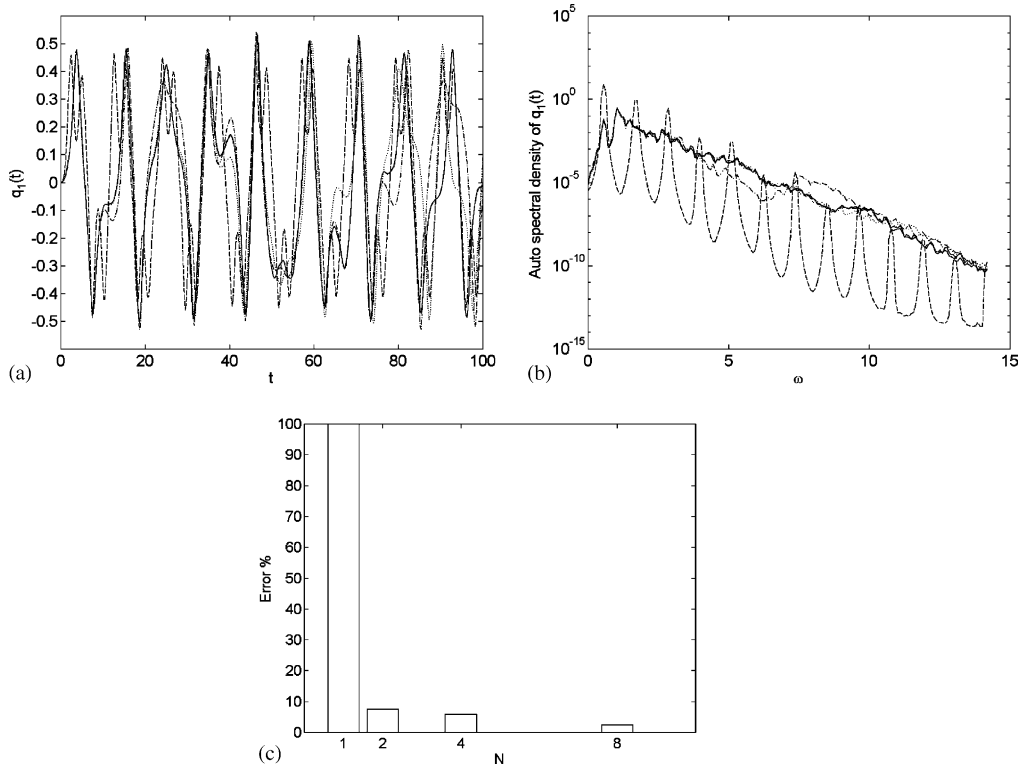

Figure 3. Chaotic motion: (a) time history for $f = 0{\cdot}54$, $\omega = 0{\cdot}567$, $v = 1{\cdot}1$; (b) power spectral densities of signals. - - - -, 1 d.o.f.; -·-·-·-, 2 d.o.f.; ····· , 4 d.o.f.; ——, $n > 4$ d.o.f.; (c) percent spectral error with respect to the 12 d.o.f. solution.

present spectra which are difficult to compare. In chaotic dynamics the sensitivity of the response to small perturbations gives rise to exponentially divergent trajectories. Moreover, the chaotic attractor probably presents a higher dimension than the regular attractor. This property of chaotic systems causes slower convergence.

It can be stated that, for the regular motion, few degrees of freedom give a good approximation, whereas in the case of chaotic dynamics the phase space must be enlarged. In the following $N = 8$ will be used for computations.

4.3. PERIODIC RESPONSE

The periodic response is investigated by means of the code *AUTO* [11]. Two excitation levels are considered: (1) $f = 0{\cdot}01$ and (2) $f = 0{\cdot}03$; the damping ratio is 0·02, and the axial speed is $v = 1{\cdot}1$ greater than v_{cr}, which belongs to the range of parameter values where the homoclinic orbit exists [2]. In Figure 4(a) for case (1) the maximum amplitude of oscillation is plotted versus the excitation frequency, normalized with the linear frequency of the system oscillating around the stable bifurcated equilibrium position ($\omega_{1,bif} = 0{\cdot}7429$). The response behavior is typical of softening type systems, in agreement with reference [6]. However, the curve presents a sharpened peak due to the strength of the non-linearity. Note that the frequency corresponding to the peak is around 30% smaller than the linear resonance. In Figure 4(b) case (2) is analyzed, the response behavior is no more

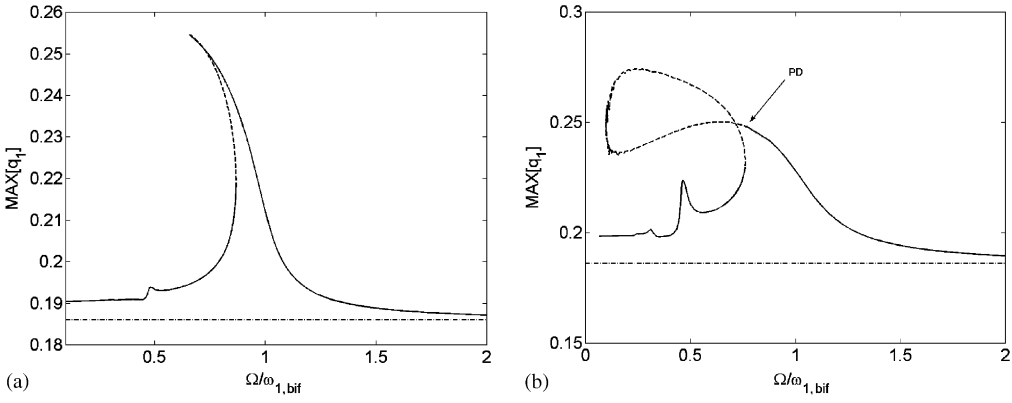

Figure 4. Amplitude frequency curve for the oscillations around the bifurcation position: (a) $v = 1{\cdot}1, f = 0{\cdot}01$; (b) $v = 1{\cdot}1, f = 0{\cdot}03$. ——, stable solution; - - - -, unstable solution; -·-·-·-, bifurcated equilibrium position; PD, period doubling.

typical, but preserves a softening character. The peak at $\omega/\omega_{1,bif} = 0{\cdot}5$ is a super-harmonic component due to the quadratic non-linearity. The presence of quadratic-like behavior deserves an explanation, since equation (1) presents cubic non-linearity only. After bifurcation, the dynamical system has more than one equilibrium position. If the governing equations are transformed through a change of co-ordinates $\bar{w} = w - w^{(1)}$, then the linearized equations furnish linear frequencies and eigenfrequencies around the bifurcated position and the non-linear part becomes quadratic and cubic. This explains the softening behavior which is typical of quadratic systems. It is interesting to note that a period doubling is found for $\omega/\omega_{1,bif} = 0{\cdot}771$: a large unstable and irregular region is present for higher amplitudes. The description of the complex behavior observed requires a deeper investigation, which includes non-stationary response analyses.

4.4. CHAOTIC DYNAMICS

The complex dynamics is analyzed via direct simulation. The time histories are initially sampled with the same frequency of the excitation. This sampling allows Poincaré sections to be obtained; they are one useful tool for analyzing chaotic responses. Moreover, bifurcation diagrams of the Poincaré maps can be drawn by varying one of the parameters which govern the response of the system. They are obtained by integrating the equation of motion for a sufficiently long time in order to eliminate the transitory motion, then a certain number of periods are considered. This procedure is repeated for different values of the parameter, using the final state of the system in the previous analysis as initial condition. The procedure allows a particular, stable, solution to be followed when a parameter is varied; a perturbation is introduced in order to force the system to fall in the most attractive orbit for each value of the parameter.

Figure 5 presents bifurcation diagrams versus the excitation amplitude with $\omega = 0{\cdot}567$ and $v = 1{\cdot}1$, as f is increased; q_1 and q_2 only are represented, even though the high-dimensional system is integrated. For very low force levels a chaotic region appears and disappears suddenly, $f \in (0{\cdot}03, 0{\cdot}056)$; after this chaotic region a periodic orbit takes place and remains stable for a large range up to $f = 0{\cdot}487$, where a cascade of bifurcations leads the system to a new chaotic region, which disappears suddenly for $f = 0{\cdot}597$. The presence of complex dynamics in the range $f \in (0{\cdot}03, 0{\cdot}056)$ is related by the loosing of stability

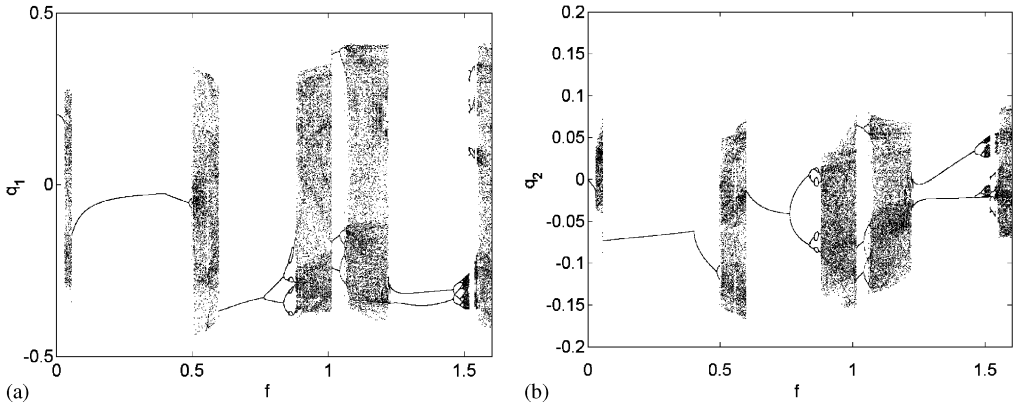

Figure 5. Bifurcation diagrams of Poincaré maps versus excitation level, $\omega = 0{\cdot}567$, $v = 1{\cdot}1$. f is increased.

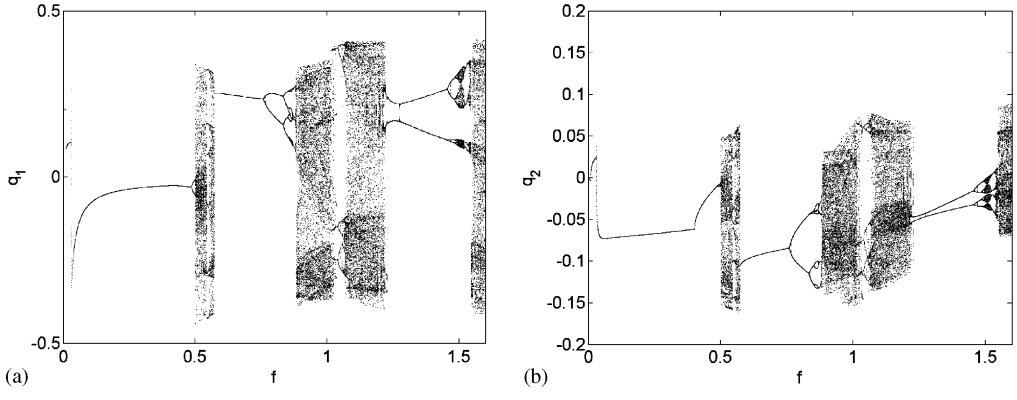

Figure 6. Bifurcation diagrams of Poincaré maps versus excitation level, $\omega = 0{\cdot}567$, $v = 1{\cdot}1$. f is decreased.

through a PD bifurcation in the amplitude–frequency curves of Figure 4(b). Here, the varying parameter is f and a different route to chaos is found.

A cascade of bifurcations, starting at $f = 0{\cdot}761$, leads to an another chaotic region, which suddenly disappears at $f = 1{\cdot}012$. A chaotic region for $f \in (1{\cdot}039, 1{\cdot}220)$ is bounded by two cascades of bifurcations and a new chaotic region at $f = 1{\cdot}460$ appears with the same modality.

A sudden disappearance of a chaotic orbit is often called blue-sky catastrophe; however, another motivation for a sudden change of dynamics can be the presence of coexisting stable chaotic and regular orbits. In order to investigate this phenomenon, the previous analysis is performed by decreasing the excitation level (Figure 6). The dynamic behavior is qualitatively the same, but two chaotic regions are changed, the first one, $f \in (0{\cdot}03, 0{\cdot}056)$ forward and $f \in (0{\cdot}03, 0{\cdot}031)$ backward, and the second one, $f \in (0{\cdot}487, 0{\cdot}597)$ forward and $f \in (0{\cdot}502, 0{\cdot}572)$ backward. In these regions it can be argued that the chaotic orbit coexists with a periodic orbit.

A second analysis is performed by changing the excitation frequency with $f = 0{\cdot}8$, $v = 1{\cdot}1$. This corresponds to a sure passage through the chaotic region, as can be observed

in Figures 5 and 6. The bifurcation diagram is presented in Figure 7; only the forward case is performed. Also in this case an intricate dynamic behavior is observed; the complexity seems to be higher than in the previous case. The cascade of bifurcations is the most frequent route to chaos, which is also present at very low frequencies. This is not a surprise, indeed the response is quite complex in the low-frequency range even for lower forces, as can be argued from Figure 4(b). The chaotic regions are the following: $\omega \in (0{\cdot}253, 0{\cdot}29)$, $\omega \in (0{\cdot}3, 0{\cdot}325)$, $\omega \in (0{\cdot}406, 0{\cdot}472)$, $\omega \in (0{\cdot}486, 0{\cdot}578)$, $\omega \in (0{\cdot}653, 0{\cdot}654)$, $\omega \in (0{\cdot}679, 0{\cdot}688)$. Only the region $\omega \in (0{\cdot}653, 0{\cdot}654)$ appears and disappears suddenly. For the remaining regions the bounds indicate the first bifurcation of the periodic orbit.

In Figure 8 the bifurcation diagram obtained by increasing the axial speed v from the sub- to the super-critical speed range is illustrated for $f = 0{\cdot}8$ and $\omega = 0{\cdot}567$. From Figure 7 it can be observed that this bifurcation diagram crosses a $2\,T$ region, where the period of the response is twice the excitation period. In fact, the only modification to the initial periodic orbit is the bifurcation into a $2\,T$ periodic orbit ($v = 1{\cdot}0529, 1{\cdot}162$). In this case the speed variation does not introduce complexity, i.e., a certain regularity of the behavior is found, indeed the same behavior is found in the backward case. In order to investigate more throughly the effect of the axial speed, a second test is performed at a slightly smaller excitation frequency ($\omega = 0{\cdot}52$) and performing a backward variation of the axial speed.

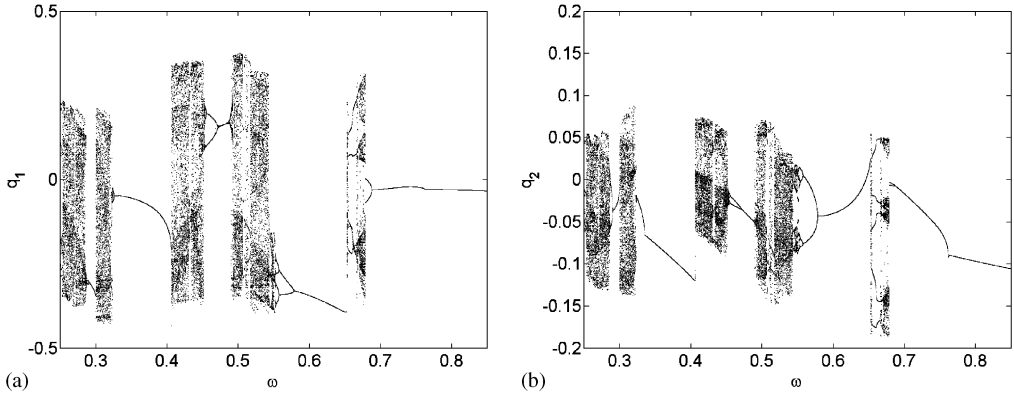

Figure 7. Bifurcation diagrams of Poincaré maps versus excitation frequency, $f = 0{\cdot}8$, $v = 1{\cdot}1$. ω is increased.

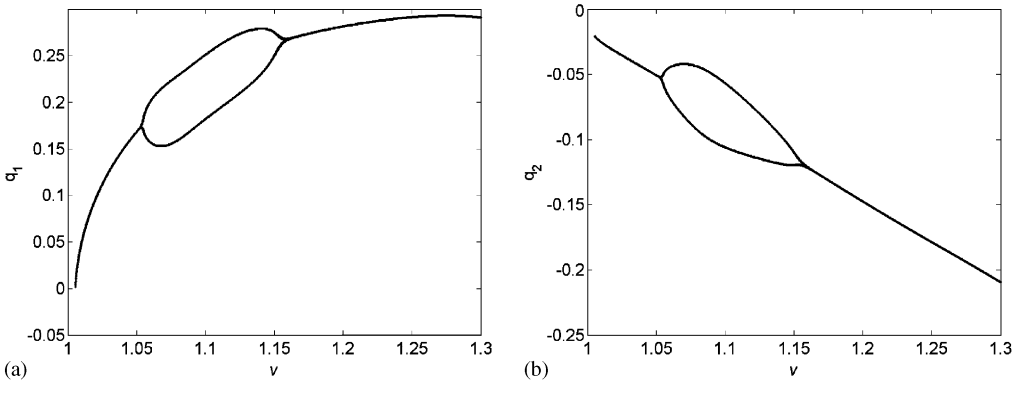

Figure 8. Bifurcation diagrams of Poincaré maps versus axial speed, $f = 0{\cdot}8$, $\omega = 0{\cdot}567$. v is increased.

The scenario is completely changed (Figure 9), the chaos dominates the dynamics, up to the proximity of the static bifurcation point, and below this point the dynamics is simply periodic. This figure confirms that even the velocity is an important parameter which governs the global dynamics of the system.

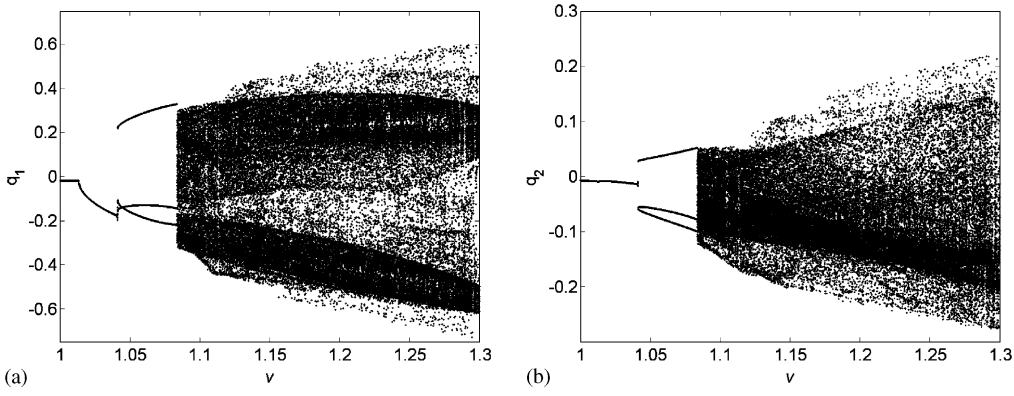

Figure 9. Bifurcation diagrams of Poincaré maps versus axial speed, $f = 0{\cdot}8$, $\omega = 0{\cdot}52$. v is decreased.

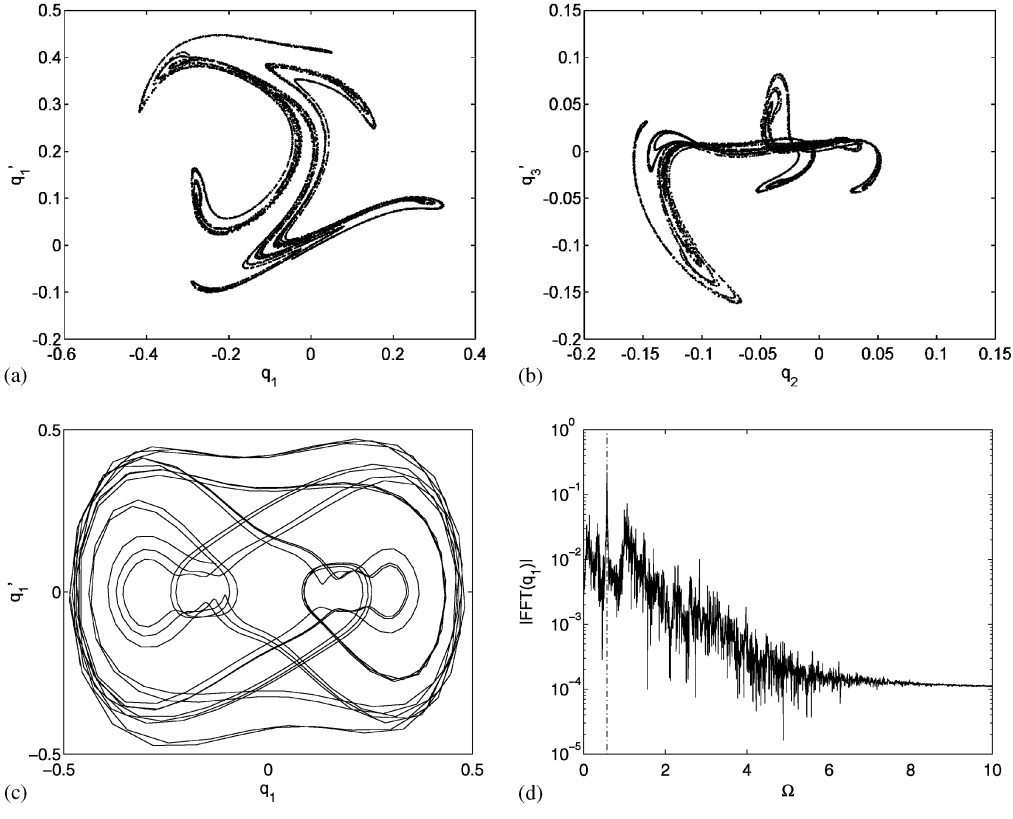

Figure 10. (a), (b) Poincaré maps; (c), (d) phase space $(q_1, \dot{q}_1)$ and spectrum of $q_1(t)$. $v = 1{\cdot}1$, $f = 0{\cdot}54$, $\omega = 0{\cdot}567$.

It is worthwhile analyzing in detail some of the previous dynamics. To this end Poicaré maps, time histories, phase space representations and Fourier spectra are presented for the most interesting cases. In Figure 10 the case $v = 1{\cdot}1$, $f = 0{\cdot}54$ and $\omega = 0{\cdot}567$ is analyzed. The Poincaré map shows that the chaotic attractor is very similar to that of a Duffing oscillator; moreover, this orbit is close to the homoclinic orbit found in reference [2]. The time history shows the non-stationary character of the dynamics and in the phase space representation, projected on the $(q_1, \dot{q}_1)$-plane, the trajectory fills the phase space. The Fourier spectrum exhibits the typical behavior of the chaotic signals, a continuous spectrum, where the most evident peak is in correspondence of the excitation frequency (dotted line), but the energy furnished at this frequency spreads over all spectrum and this reduces the response at the excitation frequency.

A similar analysis is now performed for a regular motion case, Figure 11, $v = 1{\cdot}1$, $f = 0{\cdot}75$ and $\omega = 0{\cdot}567$. An increment in the excitation amplitude with respect to the previous case makes the dynamics regular, as can be seen by the single dot in the Poincaré section (within Figure 11(a)). The phase space shows a closed trajectory and the Fourier spectrum confirms that the fundamental frequency is equal to the excitation frequency (dotted line). The global response is periodic and circumvent three equilibrium positions; the richness of non-linear field produces super-harmonics of any order, which are represented by equispaced peaks in the frequency spectrum.

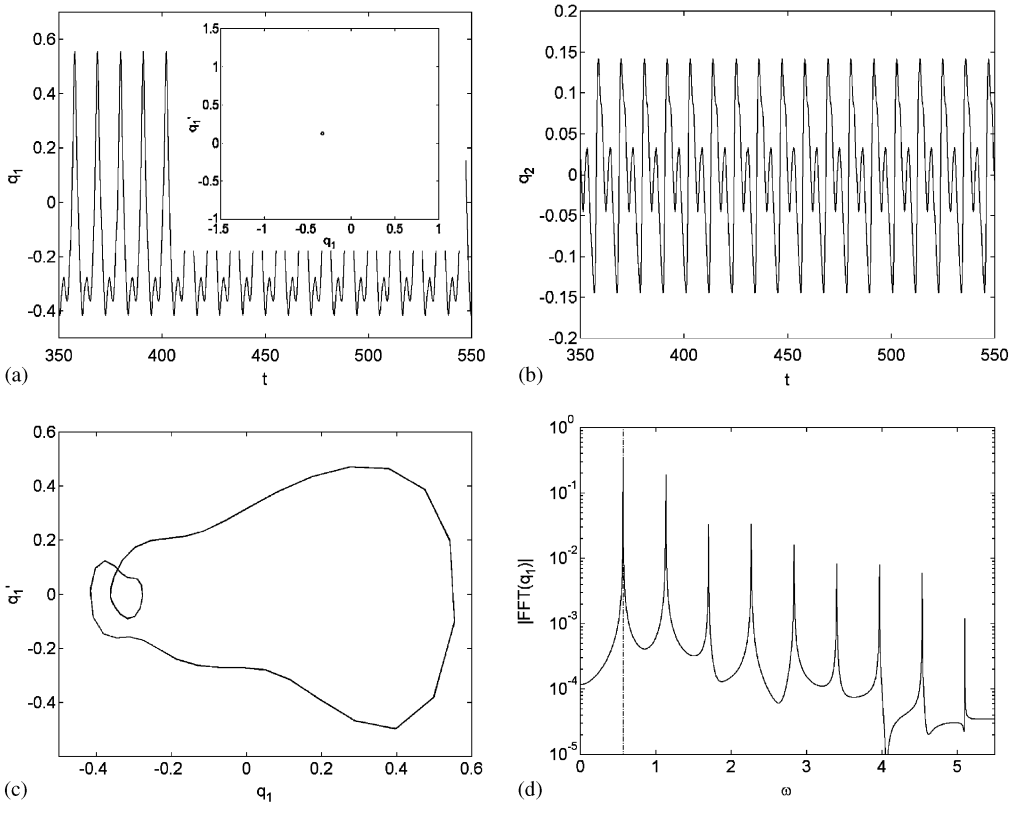

Figure 11. (a) time history of q_1 and his Poincaré map; (b) time history of q_2; (c) phase space $(q_1, \dot{q}_1)$; (d) spectrum of $q_1(t)$. $v = 1{\cdot}1$, $f = 0{\cdot}75$, $\omega = 0{\cdot}567$.

5. CONCLUSIONS

The forced response of an axially moving beam under harmonic excitation was studied in the range of velocities greater than the first critical one. A discrete high-dimensional model obtained by the Galerkin method is used to describe the dynamic deformed configuration, avoiding any constraint on the spatial shape.

The present model is compared with recent results present in the literature, showing good agreement with them. Moreover, a convergence test on the used sine series was performed. It is proved that the number of degrees of freedom used in the present work is sufficient to furnish a good spatial representation and to follow the actual dynamic behavior.

Periodic solutions are analyzed by means of the AUTO code which is able to furnish the periodic solutions and their bifurcations even if the trajectory becomes unstable. The response has been found to be of a softening type, in agreement with existing literature; however, the numerical approach made it possible investigating complicated behaviors of the amplitude frequency curves, that cannot easily be analyzed using classical perturbation techniques.

The chaotic dynamics is investigated in detail, an intricate scenario is found: cascade of bifurcations, blue-sky catastrophes and also coexisting chaotic and periodic orbits are the most interesting phenomena observed. The bifurcation diagrams presented here give an exhaustive panoramic view of the system dynamics when the main parameters are varied.

The analysis of the suitable dimension of the model to generate an accurate description of the response has shown that few degrees of freedom are sufficient in the case of regular motions and higher dimension model is required in the case of chaotic motion.

It seems that the present work enlarges the current knowledge of the dynamics of axially moving systems in the super-critical speed range. The results of numerical simulations add some contribution to the description of the system response for high axial speeds. In many mechanical applications such a situation can be real, for example in power transmission belts, magnetic tapes and many other cases. The response after the bifurcation can lead to damage in the structures and structure-borne noise, which is greatly influenced by the type of vibration; in particular, chaotic motions typically spread the energy of the vibrating system in a large frequency range. In this sense chaotic regimes can be useful because the energy spreading in a large frequency range reduces noise at a particular disturbing frequency.

ACKNOWLEDGMENT

This research has been partially supported by the Ministry for Scientific and Technological Research under grant MURST—1999/2000.

REFERENCES

1. J. A. Wickert and C. D. Mote 1988 *The Shock and Vibration Digest* **20**, 3–13. Current research on the vibration and stability of axially-moving materials.
2. F. Pellicano and F. Vestroni 2000 *Journal of Vibration and Acoustic* **122**, 21–30. Nonlinear dynamics and bifurcations of an axially moving beams.
3. R. D. Swope and W. F. Ames 1963 *Journal of Franklin Institute* **275**, 36–55. Vibrations of a moving threadline.
4. C. D. Mote Jr 1966 *Journal of Applied Mechanics* **33**, 463–464. On the non-linear oscillation of an axially moving string.

5. J. A. Wickert and C. D. Mote Jr 1990 *Journal of Applied Mechanics* **57**, 738–744. Classical vibration analysis of axially moving continua.
6. J. A. Wickert 1992 *International Journal of Non-Linear Mechanics* **27**, 503–517. Non-linear vibration of a travelling tensioned beam.
7. A. L. Thurman and C. D. Mote Jr 1969 *Journal of Applied Mechanics* **36**, 83–91. Free, periodic, nonlinear oscillation of an axially moving strip.
8. S. J. Hwang and N. C. Perkins 1992 *Journal of Sound and Vibration* **154**, 381–396. Supercritical stability of an axially moving beam. Part I: model and equilibrium analysis.
9. S. J. Hwang and N. C. Perkins 1992 *Journal of Sound and Vibration* **154**, 397–409. Supercritical stability of an axially moving beam. Part II: vibration and stability analyses.
10. F. Pellicano and F. Vestroni 1997 *Proceedings of the 16th ASME Biennal Conference, Symposium on Mechanical Vibration and Noise, Sacramento*, September 14–17, 1997. Post critical dynamics of an axially moving beam.
11. E. J. Doedel and J. P. Kerneves 1986 *Applied Mathematics Report*, *California Institute of Technology, Pasadena, CA, U.S.A.* (obtainable from doedel@cs.concordia.ca). Auto: software for continuation and bifurcation problems in ordinary differential equations.
12. J. Moon and J. A. Wickert 1997 *Journal of Sound and Vibration* **200**, 419–431. Non-linear vibration of power transmission belts.
13. F. Pellicano, A. Fregolent, A. Bertuzzi and F. Vestroni 2001 *Journal of Sound and Vibration* **244**, 669–684. Primary and parametric resonances of a power transmission belt: theoretical and experimental analysis.
14. W. Szemplinska-Stupnicka 1983 *International Journal of Non-Linear Mechanics* **18**, 149–165. Non-linear normal modes and the generalized ritz method in the problems of vibrations of non-linear elastic continuous systems.
15. C. Semler, M. P. Paidoussis 1996 *Journal of Fluids and Structures* **10**, 787–825. Nonlinear analysis of the parametric resonances of a planar fluid-conveying cantilevered pipe.
16. M. Pakdemirli, S. A. Nayfeh and A. H. Nayfeh 1995 *Nonlinear Dynamics* **8**, 65–83. Analysis of one-to-one autoparametric resonances in cables-discretization vs. direct treatment.
17. A. Steindl, H. Troger, V. Zemann 1998 *in Proceedings of the IUTAM Symposium on Nonlinear and Chaotic Dynamics in Mechanics* (F. C. Moon, editor). Dordrecht: Kluwer Academic Publ. Improved Galerkin methods for the dimension reduction of nonlinear dynamical systems.
18. F. Pellicano and F. Zirilli 1998 *International Journal of Non-Linear Mechanics* **33**, 691–711. Boundary layers and nonlinear vibrations of an axially moving beam.
19. R. K. Jha and R. G. Parker 2000 in *Vibration and Control of Continuous Systems, Proceedings of the ASME International Mechanical Engineering. Congress and Exposition* (C. D. Rahn and J. A. Wickert, editors), DE-Vol. 107, New York: ASME. Spatial discretization of axially moving media vibration problems.